Analytical Biochemistry **289,** 173–186 (2001)
doi:10.1006/abio.2000.4920, available online at http://www.idealibrary.com on IDEAL®

Fast Transient Cytokine–Receptor Interactions Monitored in Real Time by Reflectometric Interference Spectroscopy

Jacob Piehler[1] and Gideon Schreiber
Department of Biological Chemistry, The Weizmann Institute of Science, 76100 Rehovot, Israel

Received June 6, 2000

Investigating protein–protein interactions by mutational analysis requires practical techniques for quantifying rate constants and equilibrium constants over several orders of magnitude with reasonably high sample throughput. We have employed spectroscopic interferometry for label-free monitoring of the interaction between the cytokine interferon α2 (IFNα2) and the extracellular domain of its receptor ifnar2 (ifnar2-EC). We implemented a versatile surface chemistry for the glass substrate of this transducer for covalent immobilization of proteins. Affinity capturing with a monoclonal anti-ifnar2-EC antibody (mAb) followed by crosslinking with a second, noncompetitive mAb provided stable, but still reversible, immobilization of ifnar2-EC. We measured kinetics and affinity of numerous of mutants of IFNα2 and ifnar2-EC. Dissociation rate constants up to 0.3 s^{-1} and association rate constants up to 3×10^6 M^{-1} s^{-1} were resolved by the system. Dissociation constants down to 200 μM were measured with protein concentrations up to 50 μM without no background signal or nonspecific binding. The instrument detection limit is ~10 pm without the need for temperature stabilization or referencing channels. The system proved effective for large-scale mutational analysis involving alanine scanning mutagenesis and double mutant cycles. © 2001 Academic Press

Key Words: **label-free detection; surface chemistry; protein immobilization; protein–protein interactions; type I interferon receptor.**

Specific recognition of growth factors, hormones, or cytokines at cell surface receptors triggers signal transduction into the cell. Systematic design of antagonists and agonists for such receptors requires understanding of these interactions on a structural and thermodynamic level. With an increasing number of receptors being discovered and cloned, techniques for characterizing these interactions are tremendously gaining importance. Mutational analysis in combination with biophysical characterization is the method of choice to probe protein–protein interactions on a functional level. By alanine scanning mutagenesis, energetic contributions of groups or individual amino acid residues to the complex stability can be quantified (1–3). Double or multiple mutant cycle analysis enables probing free energy and cooperativity of interactions between individual amino acid residues (4, 5). For these investigations, however, changes in affinity and kinetics of complex formation upon mutation must be measured accurately. Both subtle effects and changes in affinity over several orders of magnitude must be quantified with reasonably high throughput and moderate sample consumption.

Label-free solid-phase detection has proved to be a versatile tool in biomolecular interaction analysis (BIA).[2] Surface plasmon resonance (SPR) and other techniques based on evanescent field interrogation have been employed to monitor binding to immobilized compounds, thus giving access to thermodynamics and kinetics of the interaction (6–8). The heterogeneous-phase format facilitates sample handling and automatization and effectively limits sample consumption. However, immobilization of proteins is required, which can substantially affect

[1] To whom correspondence should be addressed at current address: Institut für Physiologische Chemie, Klinikum der Philipps-Universität Marburg, Karl-von-Frisch-Strasse 1, D-35033 Marburg, Germany. Fax: 49 (0) 6421 286 4335. E-mail: piehler@mailer.uni-marburg.de.

[2] Abbreviations used: ifnar, type I interferon receptor; IFN, interferon; mAb, monoclonal antibody; EC, extracellular domain; EDC, ethyl-dimethylaminpropyl carbodiimide; NHS, *N*-hydroxy-succinimide; SPR, surface plasmon resonance; PEG, poly (ethylene glycol); RIfS, reflectometric interference spectroscopy; AMD, amino-functionalized dextran; CD, carboxyl-functionalized dextran layer; BIA, biomolecular interaction analysis; BSA, bovine serum albumin; IgG, immunoglobulin; wt, wild type; mut, mutant; ifnar2-EC-bi, biotinylated ifnar2-EC; GOPTS, glycidyloxipropyltrimethoxysilane.

0003-2697/01 $35.00

kinetics and thermodynamics of the interaction. Thus, appropriate surface modification for a functional immobilization of proteins remains a critical task, which must be individually optimized and validated for each system. While absolute kinetic and thermodynamic parameters often do not agree with data from homogeneous-phase methods (9), solid-phase detection has proved to be very reliable for mapping relative changes upon mutation (1, 3). Extensive mutational analysis of a binding site including double and multiple mutant cycles requires vast numbers of measurements, exponentially growing with the subset of mutants being investigated. Immobilization techniques for stable, but reversible, affinity capturing could effectively facilitate mutational analysis. Established systems such as antibodies or metal chelates interacting with His_6-tagged proteins do often leak out considerably (10) and are therefore of limited benefit for extensive screening. Further limitations of label-free solid-phase detection arise from high background signals for two reasons: first, owing to the mass-sensitive detection, specific interactions cannot be discriminated from nonspecific adsorption to the surface. Second, composition and refractive index of the sample affect the signal, in particular, in evanescent field interrogation such as SPR. Both nonspecific binding and bulk refractive index increase with sample concentration. Thus, sophisticated instrumentation with referencing and temperature stabilization is required for detecting binding affinities in the micromolar range (11).

In contrast to evanescent field interrogation, reflectometric techniques such as ellipsometry or interferometry selectively probe physical layers attached to a surface (12). Reflectometric interference spectroscopy (RIfS) has successfully been employed for time-resolved detection of biomolecular interactions (13, 14), with detection limits of a few picograms per square millimeter (15). Here, we describe the application of RIfS for label-free monitoring of protein–protein interactions. Suitable and versatile surface chemistry for covalent attachment of proteins onto the silica surface of the transducer was developed and thoroughly characterized. Different strategies were investigated to immobilize the extracellular domain of the type I interferon receptor ifnar2 (ifnar2-EC) for monitoring the binding of interferon $\alpha 2$ (IFNα2) in real time. Using numerous mutants of IFNα2 and ifnar2-EC, we measured rate constants up to 0.3 s^{-1} and dissociation constants up to at least 200 μM with high accuracy without the need for referencing background effects.

MATERIALS AND METHODS

Materials

GOPTS and sodium periodate were purchased from Fluka, dextrans and glutaric anhydride were from Sigma, and sodium cyanoborohydride was from Aldrich. Carboxy-functionalized polyethylene glycol (PEG) (2000 g/mol) was from Rapp Polymere (Tübingen, Germany). Amino-functionalized dextrans of different molecular mass (M_r of 39.5 and 476 kg/mol, termed AMD40 and AMD500, respectively, in the following) were prepared by diol oxidation followed by reductive amination. In 38 ml water, 2 g (12 mmol anhydroglucose units) dextran was dissolved and reacted with 287 mg (1.35 mmol) sodium periodate at 4°C for 7 h. After dialysis against water, 10 ml (167 mmol) ethanolamine adjusted to pH 8.0 and 1.5 mg (24 mmol) sodium cyanoborohydride were added. After 12 h at room temperature, an additional 1 mg (1.6 mmol) sodium cyanoborhydride was added. After an additional 12-h reacting period, the solution was extensively dialyzed against 25 mM 4-morpholinepropanesulfonic acid, pH 7.5. The dextran was precipitated by adding the eightfold volume of methanol, filtered on a sintered glass funnel, and washed with methanol.

Human IFNα2 and ifnar2-EC expressed in *Escherichia coli* were refolded and purified to homogeneity as described earlier (16). Amino acid residues in the binding site were mutated to alanine by site-directed mutagenesis as described (3, 17). Solutions of IFNα2 were concentrated up to 1–3 mM using Fugisep spin concentrators (Intersep, UK). Ifnar2-EC at 20 μM concentration was biotinylated by reaction with a twofold molar excess of biotin amidocaproate *N*-hydroxysuccinimide in 20 mM Hepes, pH 7.2, for 12 h at 4°C. Monoclonal anti-ifnar2-EC antibodies 46.10 and 117.7 purified by fractionated ammonium sulfate precipitation were a gift from D. Novick, The Weizmann Institute of Science.

Surface Modification

Carboxyl-functionalized dextran layers (CD40 and CD500, obtained from AMD40 and AMD500, respectively) were prepared by a three-step chemical modification of the silica surface of the transducer. Prior to silanization, the substrate surface was cleaned by treatment with 3 M sodium hydroxide for 5 min followed by incubation with a freshly prepared piranha solution (60% concentrated sulfuric acid and 40% of a 30% hydrogen peroxide solution) for 1 h. After rinsing with water, the surface was dried in a nitrogen stream. The surface was silanized by incubating pure GOPTS (5 $\mu l/cm^2$) at 75°C for 15 min, avoiding exposure to the atmosphere by assembling two slides face to face. The slides were allowed to cool down to room temperature for 15 min, washed with dry acetone, and dried in a nitrogen stream. On the freshly silanized surface, 5 $\mu l/cm^2$ of a solution of 1 mg AMD in 2 μl water was incubated for 24 h in a water-vapor-saturated chamber with two surfaces being assembled face to face. The slides were thoroughly rinsed with water and dried in

a nitrogen stream. To introduce carboxylic groups into the dextran layer, ~50 mg glutaric anhydride was molten on the surface at 75°C for 2 h in a face-to-face assembly, rinsed with water, and dried with nitrogen. These slides were stored for several weeks without any significant loss in binding capacity. Carboxy-terminated high-density PEG layers were prepared from α,ω-dicarboxy PEG (2000 g/mol) as described earlier (18). AMD (1 mg in 2 μl water) was coupled to the exposed carboxyl groups of these layers by amide coupling using the water-soluble carbodiimide EDC and subsequently reacted with glutaric anhydride as described above. These surfaces are referred to as PCD40 and PCD500 according to the molecular weight of the AMD coupled to the PEG.

Ellipsometry

Surface loading of the dextran layers before and after coupling of glutaric anhydride was determined by ellipsometry using a null ellipsometer (AutoEL, Rudolph Research, Flanders, NJ) with a He–Ne laser light source, $\lambda = 632.8$ nm, and an angle of incidence at 70°. The refractive index was assumed to be 1.5 for all deposited layers in a three-phase model "substrate/organic layer/air." An average of measurements at three spots of a sample gave the resulting thickness of the layer, and three samples were measured. The thickness of the native silica layer on the surface of the silicon was measured after treatment with piranha solution and was found to be between 1.1 and 1.5 nm. The surface loading was estimated from the layer thickness assuming a density of 1.2 g/cm^3 corresponding to the refractive index of 1.5 (19).

Contact Angles

Advancing and receding contact angles were measured with a goniometer (NRL 100, Ramé-Hart, Mountain Lakes, NJ) using fresh ultrapure water (MilliQ, Millipore AB, Sweden) in laboratory atmosphere. The samples were taken from the same batches as for the ellipsometric measurements. One measurement of the advancing and receding contact angle was done per sample; results from four to five samples were averaged.

RIfS Measurements

Interactions of proteins with the surface were monitored by RIfS (20). The principles and the experimental setup of this technique for monitoring binding events at interfaces were discussed in detail previously (13, 16). The apparent optical thickness of a thin silica layer (500–600 nm) is determined by white light interference. Changes in thickness upon protein binding at the surface of this layer are monitored as a shift of an extremum of the interference spectrum (Fig. 1A). The setup schematically depicted in Fig. 1B was realized by modifying a commercial, diode-array-based spectrophotometer (Spekol 1100, AnalytikJena, Germany) as described earlier (14). The transducer slides (custom-made by Schott, Germany) were mounted in a flow cell with a 1-mm-wide and 0.05-mm-deep flow channel. Sample handling was carried out with a dual syringe device (Microlab 541C, Hamilton, Switzerland), combined with a distribution valve (MVP, Hamilton, Switzerland) and an autosampler (Remote 50KK, Ismatec, Switzerland). The software "Measure" (G. Kraus, Novartis, Switzerland) was used for synchronized control and data acquisition. Binding curves $R(t)$ were recorded as shift of the minimum of the reflectance spectrum (order 1.5 at ~560 nm) vs time with a time resolution of 1 s. A change of the surface loading of 1 ng/mm^2 protein leads to a shift $R \approx 1$ nm, corresponding to ~1000 RU of the Biacore system (unpublished results). All binding curves were corrected by subtracting a blank run averaged from two to four measurements.

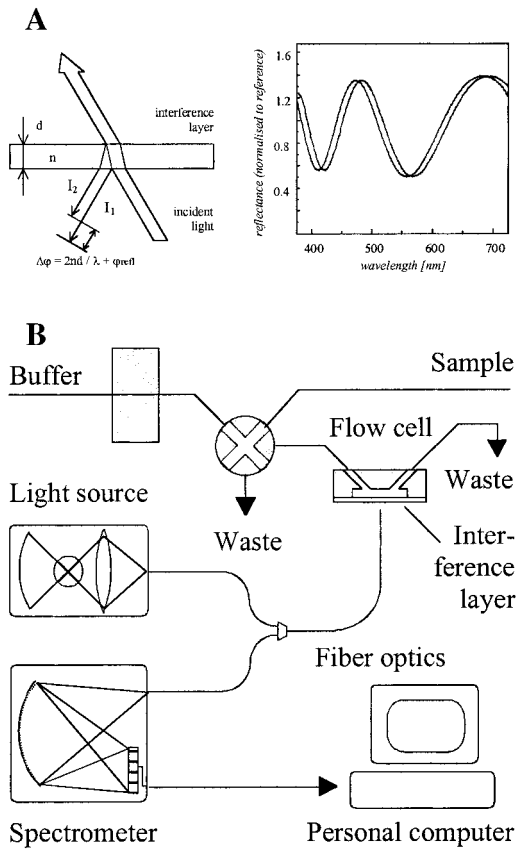

FIG. 1. Principle and implementation of reflectometric interference spectroscopy. (A) The interference pattern of a thin layer is shifted upon binding to this layer. The shift of the interference minimum at ~560 nm is monitored with time. (B) Experimental setup for measuring protein–protein interactions with RIfS.

All measurements were carried out in buffer containing 20 mM Hepes, 150 mM NaCl, and 0.01% Triton X-100 with a pH of 7.5 at room temperature (~23°C). Proteins were covalently immobilized by amide coupling chemistry. Carboxyl groups were activated by a 30 s pulse of freshly prepared solution 0.1 mM NHS and 0.0375 mM EDC. To enhance coupling by electrostatic preconcentration, ifnar2-EC was diluted into 10 mM sodium acetate, pH 4.2, and antibodies and streptavidin were diluted into 10 mM sodium acetate, pH 4.9. Protein solutions were injected at 1 μl/s for 2 min and were incubated for an additional 2 min at stopped flow. After rinsing, 1 M dimethylaminopropylamine was injected for 2 min to remove residual activated groups. For BIA experiments, protein stock solutions were diluted at least 40-fold into the running buffer prior to injection. Sample volumes of 500 μl were filled into the sample tubing, being separated from the flow buffer by an 500-μl air segment. The samples were injected with a speed of 25 μl/s for 10 s, followed by an additional 125 s at 1 μl/s. After injection, the residual sample was discarded and the flow cell was rinsed with buffer at 25 μl/s. Nonspecific adsorption at the surface was investigated by incubating 1 mg/ml BSA. Electrostatic preconcentration was investigated with 20 μg/ml IFNα2 in 10 mM acetate, pH 4.7, and with 50 μg/ml sheep IgG in 10 mM acetate, pH 4.9.

Data Analysis

By flowthrough detection, the concentration of the binding ligand is maintained constant, thus providing pseudo-first-order conditions. Association and dissociation rate constants (k_a and k_d) were determined from the binding curves by fitting the model for a simple 1:1 interaction using the program BIAeval 2.1 (Biacore AB, Sweden). Dissociation constants K_D were determined either from the rate constants according to

$$K_D = \frac{k_d}{k_a} \qquad [1]$$

or from the equilibrium response R_{eq} at different concentrations c by fitting the law of mass action

$$R_{eq} = R_{max} \frac{c}{K_D + c} \qquad [2]$$

with R_{max} being the maximum response. The parameters K_D and R_{max} were fitted, when the total amplitude was covered with data points. At low binding affinities ($K_D > 10$ μM), maximum R_{eq} were lower than 75% of R_{max}, and the value for R_{max} taken from a mutant with higher affinity was fixed and only K_D was fitted. Diffusion rate constant k_{diff} and the diffusion layer thickness δ were determined from diffusion controlled electrostatic binding according to the [1] Fickian law

$$J(x) = -D \frac{c_0 - c}{\delta} = k_{diff}(c_0 - c_s) \qquad [3]$$

with the diffusion coefficient D, the bulk concentration c_0, and the surface concentration c_s, assuming that $c_0 - c_s \approx c_0$ (21).

Changes in interaction energy upon mutation were calculated from the dissociation constants K_D and from dissociation rate constants k_d of wild-type (wt) and mutant (mut) proteins according to

$$\Delta\Delta G^0_{K_D} = RT \ln \frac{K_D^{mut}}{K_D^{wt}} \qquad [4]$$

and

$$\Delta\Delta G^{\ddagger}_{k_d} = RT \ln \frac{k_d^{mut}}{k_d^{wt}} \qquad [5]$$

as described in detail previously (17).

RESULTS

Surface Modification and Characterization

Carboxyl-functionalized dextran layers obtained from different AMD and different coupling strategies were characterized with respect to surface loading, nonspecific binding, and electrostatic preconcentration of proteins. After all coupling reactions, the surfaces remained clear without any visible heterogeneity. The attachment of AMD by directly coupling to GOPTS-activated surfaces was characterized by ellipsometry and contact angle measurements (Table 1). After coupling AMD500 and AMD40, a surface loading of 2.2 and 1.0 ng/mm^2, respectively, was observed. The comparably low wetting by water on the GOPTS-treated surface ($\Theta_{ad} = 48°$ (18)) changed to complete wetting by water after coupling the AMD. During reaction with glutaric anhydride, the surface loading increased by an additional 2.6 ng/mm^2 for AMD500 and 1.4 ng/mm^2 for AMD40, respectively. From the molecular masses of the anhydroglucose monomer unit (162 g/mol) and the monoglutarate moiety (114 g/mol), the concentration of carboxylic groups is estimated to be 1.7 per anhydroglucose group in the CD500 and 2.4 in the CD40. The wetting of the surfaces decreased substantially after reaction with glutaric anhydride, with contact angles Θ_{ad} of 37° for CD40 and 44° for CD500, probably due to the hydrophobic aliphatic backbone of the glutaric anhydride. The high hysteresis of 14° for CD40 and 21° for CD500, respectively, indicates high flexibility of the

TABLE 1

Surface Analysis by Ellipsometry and by Contact Angle Measurements after Coupling of AMD and Reaction with Glutaric Anhydride (GA)

Surface	AMD[a] (ng/mm^2)	GA[a] (ng/mm^2)	Molar ratio[b]	Θ_{ad} (°)[c]	Θ_{re} (°)[c]	H (°)[c]
CD40	1.0 ± 0.2	1.4 ± 0.2	1.7	37 ± 2	23 ± 2	14 ± 2
CD500	2.2 ± 0.2	2.6 ± 0.2	2.4	44 ± 2	23 ± 2	21 ± 2

[a] Estimated from the ellipsometrically determined thickness of the dextran layer.
[b] Average number of monoglutarate moieties per anhydroglucose monomer unit of the dextran.
[c] Wetting by water, determined after reaction with glutaric anhydride.

dextran layers, which increased with the molecular mass of the dextran. On PEG-modified surfaces, less change in wetting upon coupling of AMD was observed, indicating that less dextran was attached by this method. However, surface loading and wetting were not quantified for these layers.

Data Correction, Time Resolution, and Detection Limits

Protein binding to the surfaces was monitored by RIfS in a flowthrough system. Typical blank runs with only running buffer in the sample injected on CD500 and CD40 surfaces with immobilized protein are shown in Fig. 2A. Changes in the flow rate during loading of the sample, injection, and rinsing clearly affected the signal. The exact reasons for this effect are not clear, but a significant dependence on the surface chemistry was observed: the larger the dextran and the more protein was immobilized, the stronger were the amplitudes of changes upon changing the flow rates (cf. Fig. 2A). To eliminate such perturbations of the signal, all binding curves were corrected by subtracting a blank run, which was regularly measured throughout the experiments. It must be emphasized that these blank runs exclusively correct for system parameters, not for background related to the sample. One of the blank runs on CD500 shown in Fig. 2A after correction with a second blank run is shown in Fig. 2B. The root mean square noise of the system at 1 Hz spectra acquisition was determined from a linear fit of this curve to be <2 pm for all curves investigated. Thus, changes in surface loading down to 10 pm corresponding to ~10 pg/mm^2 can be clearly detected by the system. The drift determined from the linear fit of the corrected blank runs was <0.01 pm/s for all curves investigated and is therefore negligible for binding curves carried out within a few hundred seconds. It must be mentioned, however, that other, nonstatistical parameters such as instabilities due to sample handling can also affect the actual detection limit in an individual experiment.

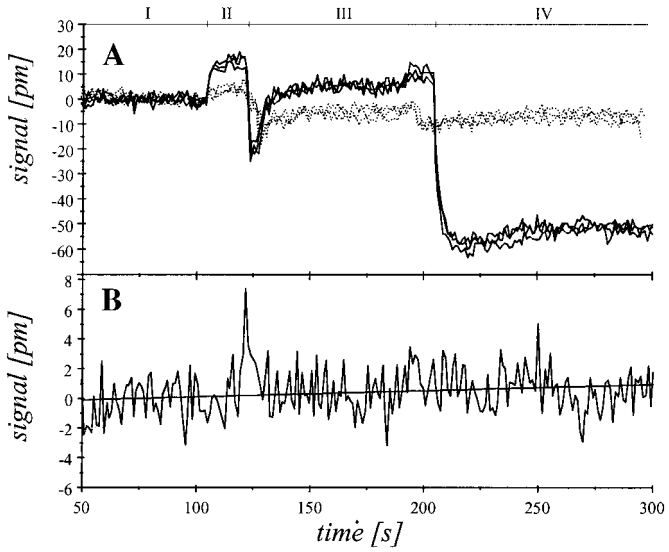

FIG. 2. Data correction and detection limits. (A) Blank runs, i.e., injections of the running buffer, on CD500 (—) and CD40 (···) with immobilized protein, three consecutive curves for each surface. The cycle includes the preinjection baseline (I), loading of the sample (II), injection (III), and rinsing (IV). (B) One of the blank runs on CD500 shown in A after correction with a second blank run and a linear fit over the corrected sensorgram.

The time resolution in solid-phase detection is typically limited by the sample handling, i.e., by the time needed to exchange the sample in the flow cavity. The times for rise and fall of the sample concentration were measured by injecting 1 M NaCl in the same buffer as the running buffer. A representative set of three consecutive injections of this solution is shown in Fig. 3A. Within 3 s, the maximum concentration is reached with a mean rate constant of 1.7 s^{-1} as determined by an exponential fit (Fig. 3B). During rinsing, the sample was completely removed within 3 s with a time constant of 1.1 s^{-1} (Fig. 3C). Thus, rate constants up to ~0.3 s^{-1} for both association and dissociation can be determined with this system.

Functional Properties and Mass Transport Limitation

Nonspecific binding as well as the capacities and the rates of electrostatic binding at the CD layers are summarized in Table 2. All CD-modified surfaces showed less than detectable nonspecific binding during incuba-

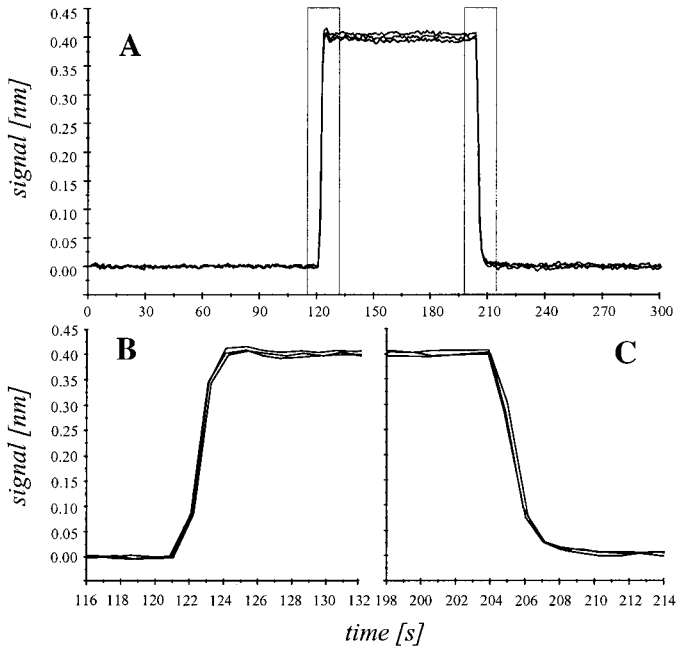

FIG. 3. Determination of the time resolution as defined by the rise and fall times of sample concentration in the flow cell. (A) Concentration profile measured by injecting the running buffer containing 1 M NaCl (overlay of three consecutive runs). (B and C) Enlarged views of the rise and fall regions of the injection, respectively, as indicated by the boxes in sensorgram A.

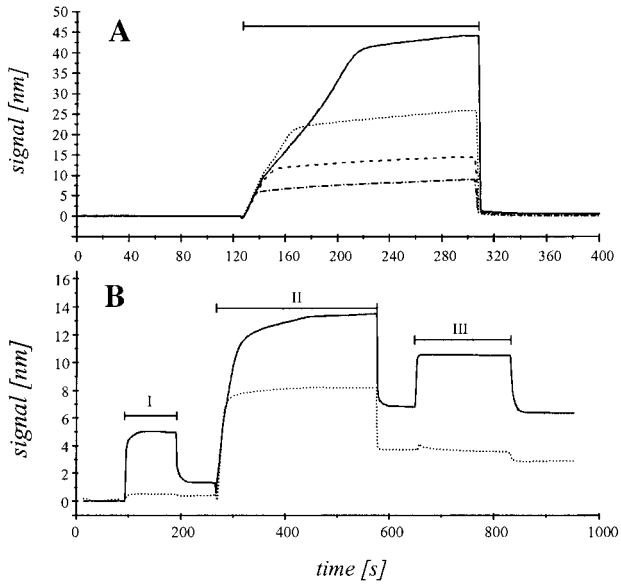

FIG. 4. (A) Preconcentration of IgG in 10 mM acetate, pH 4.9, on CD500 (—), PCD500 (···), CD40 (- - -), and PCD40 (·-·-·). The bar indicates the injection period. (B) Protein immobilization by amide coupling chemistry including activation (I), coupling (II), and deactivation (III). The two curves are typical examples for the immobilization of ifnar2-EC on CD500 (—) and of mAb 46.10 on CD40 (---). Note the different background signal during activation and deactivation on the two different surfaces.

tion of 1 mg/ml BSA at physiological ionic strength and pH (less than 20 pm during the total incubation time). At low ionic strength and a pH below the p*I* of the proteins, strong electrostatic binding of proteins to the CD surfaces was observed as shown in Fig. 4A for sheep IgG on different surfaces. The preconcentrated proteins were completely removed during rinsing with buffer of physiological pH and ionic strength. The binding capacities of the surfaces varied between different proteins, as well as the molecular mass of the coupled dextran and the coupling method. Higher binding capacity was observed for AMD of higher molecular mass and for AMD directly coupled to the silanized surface compared to AMD coupled via a PEG layer. Thus, the binding capacity of the surface can be controlled with the amount of attached dextran, as we have shown before for antibody–hapten interactions (19).

The rates of electrostatic binding were linear over the first 50% of the maximum binding amplitude, indicating mass transport limitation due to very fast electrostatic association. These mass transport limited rates were ~350 pm/s for IFNα2 (20 μg/ml) and ~640 pm/s for IgG (50 μg/ml) at a flow rate of 5 μl/min for all

TABLE 2

Functional Properties of Differently Modified Surfaces

	IFNα2[a]		IgG[b]		BSA[c]
Surface	Max[d] (nm)	Slope[e] (pm/s)	Max[d] (nm)	Slope[e] (pm/s)	Max[d] (pm)
CD40	6.4 ± 0.5	360 ± 20	14 ± 1	630 ± 20	<20
CD500	31 ± 2	370 ± 20	42 ± 3	640 ± 20	<20
PDX40	4.5 ± 0.3	350 ± 20	9.1 ± 0.5	640 ± 20	<20
PDX500	15 ± 1	370 ± 20	25 ± 2	650 ± 20	<20

[a] 20 μg/ml IFNα2 in 10 mM acetate, pH 4.7.
[b] 50 μg/ml sheep IgG in 10 mM acetate, pH 4.9.
[c] 1 mg/ml BSA in 20 mM Hepes, pH 7.5, 150 mM NaCl, and 0.01% Triton X-100.
[d] Maximum binding after a 180-s injection period.
[e] Slope of the binding curve at 5 μl/s injection flow rate.

surfaces. For CD500 layers, though, significant decrease in the binding rate followed by another increase was observed (Fig. 4). Since the interferometric shift increases linear with the surface loading (unpublished results), the shape of the curve suggests that substantial rearrangement of the layer takes place during binding. Assuming a diffusion coefficient of $D = 5 \times 10^{-11}$m^2/s for IgG, the diffusion layer thickness δ is estimated to be 5–10 μm. The diffusion rate constants k_{diff} for the proteins are 1.3×10^{-5} m/s for IgG and 1.8×10^{-5} m/s for IFNα2. For measuring association kinetics of biomolecular interaction at the surface, the maximum rate of the protein–protein association $L = k_a \cdot \Gamma_{\max}$ should not exceed the maximum diffusion rate k_{diff} (21). At a typical maximum binding of 200 pg/mm^2 IFNα2, L is $1 \cdot 10^{-5}$ m/s for an association rate constant of 1×10^6 M^{-1} s^{-1}. Thus, maximum association rate constants of $1–5 \times 10^6$ M^{-1} s^{-1} can be determined with this system, depending on the molecular mass of the protein and the surface loading.

Immobilization of Ifnar2-EC

Stable immobilization of ifnar2-EC without affecting its functional properties is a prerequisite for assessing accurate parameters of affinity and kinetics of large numbers of different mutants. Three different techniques for immobilizing ifnar2-EC were investigated: (i) amine-selective, covalent coupling; (ii) binding of biotinylated ifnar2-EC to immobilized streptavidin; and (iii) affinity capturing with monoclonal anti-ifnar2-EC antibodies.

Proteins were covalently coupled to CD after activating the carboxylic groups with EDC/NHS as established for other biosensor systems (22). The coupling efficiency of the glutaric acid residues, however, proved to be higher than the α-oxyacetic acid groups typically used in biomolecular interaction analysis. Therefore, a fivefold lower concentration of the activating reagent EDC was used (37.5 mM), while a higher concentration of NHS was applied to avoid possible transesterification. Sensorgrams of immobilization including activation, coupling at low ionic strength and pH below the pI of the protein as well as deactivation of the remaining active esters are shown in Fig. 4B. Interestingly, the background signals during activation and deactivation are substantially stronger for CD500 compared to CD40, suggesting that the background strongly increases with the protein-binding capacity of the interfacial layer. Ifnar2-EC was typically coupled to CD500 layers (Fig. 4B), irreversibly immobilizing 4–6 nm of protein. However, only a minor fraction of the immobilized protein (5–10%) was active, binding a maximum of 200–350 pm IFNα2 (Fig. 5A). The fraction of active protein varied between different ifnar2-EC mutants, and some mutants (W74A, E79A, and D106A) completely lost their activity. Wild-type ifnar2-EC lost ~75% of its activity during 1 day. The main drawback of this immobilization method, however, was the fact that the maximum loading $R_{\max}$ was different for different mutants of IFNα2, decreasing with decreasing affinity (Fig. 5A). Apparently, covalent coupling below the pI resulted in species with different affinity (cf. below).

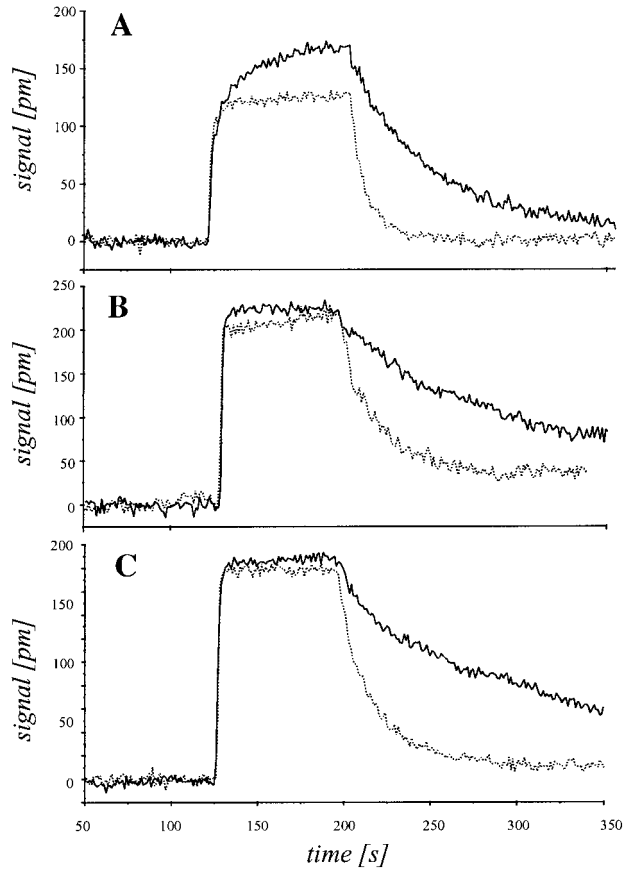

FIG. 5. Kinetics of binding of IFNα2 wt (—) and the mutant L26A (···) to differently immobilized ifnar2-EC. (A) Ifnar2-EC directly immobilized to the surface by amide coupling with electrostatic preconcentration (CD500). (B) Biotinylated ifnar2-EC captured by covalently immobilized streptavidin (CD500). (C) Ifnar2-EC captured with immobilized mAb 46.10 and crosslinked by mAb 117.7.

Biotinylated ifnar2-EC (ifnar2-EC-bi) was captured with streptavidin immobilized on CD500 (~5 ng/mm^2). Approximately 300–500 pm ifnar2-EC-bi was attached irreversibly (data not shown), binding a maximum of 200–300 pm IFNα2 (Fig. 5B). Thus, approximately 75% of the receptor was functionally immobilized under these conditions. Comparing binding of different IFNα2 mutants showed that in contrast to the direct coupling procedure the same maximum loading $R_{\max}$ was obtained (Fig. 5B). Furthermore, immobilized ifnar2-EC-bi was significantly more stable, with a loss of ~20% binding capacity per day.

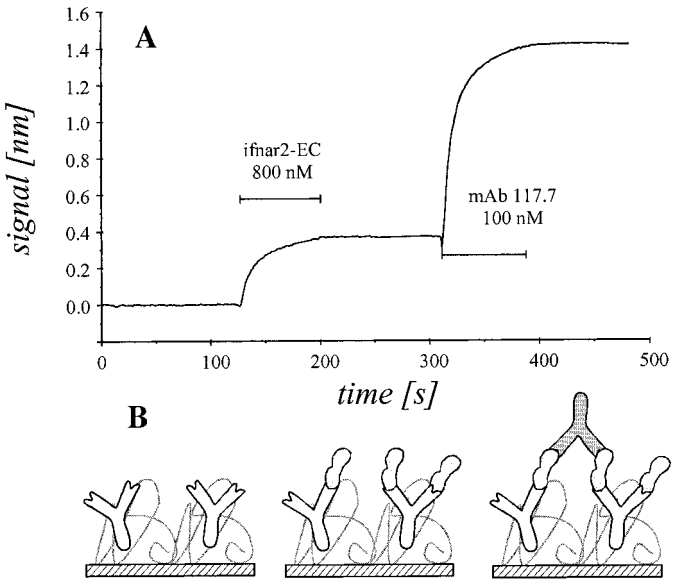

FIG. 6. Immobilization of ifnar2-EC by affinity capturing. (A) Binding curve for capturing ifnar2-EC with immobilized mAb 46.10, followed by crosslinking with mAb 117.7. (B) Schematic illustration of the immobilization procedure.

To reversibly immobilize ifnar2-EC by affinity capturing, a monoclonal antibody raised against soluble ifnar2-EC, which does not neutralize IFN activity (monoclonal antibody (mAb) 46.10 (23)) was covalently coupled to CD40 surfaces (Fig. 4B). Typically, 2.5–3 nm of antibody was immobilized, which specifically bound 400–500 pm ifnar2-EC (Fig. 6). Taking the relative molecular mass of the proteins into account (25 kDa for ifnar2-EC, 75 kDa per binding site of the antibody), approximately 40–50% of the immobilized antibody was binding ifnar2-EC. This is in the range expected for an antibody preparation purified only by ammonium sulfate precipitation, indicating that most of the antibody remained active during immobilization. Dissociation of the captured ifnar2-EC was very slow, with a dissociation rate constant $k_d < 1 \times 10^{-4}$ s^{-1}. During binding experiments, however, significant leaking out was observed, with a loss in binding capacity of ~5% per injection. To improve the stability, we used the avidity of a second, noncompetitive mAb for crosslinking ifnar2-EC after capturing it on the surface as schematically depicted in Fig. 6B. Immediately after capturing ifnar2-EC with mAb 46.10 immobilized on the chip, the second anti-ifnar2-EC mAb (117.7 (23)) was injected (Fig. 6A). This antibody does not affect binding of IFN and binds ifnar2-EC noncompetitive to 46.10 with a dissociation rate constant of 2×10^{-3} s^{-1} when immobilized on the surface. As a second antibody, however, 117.7 bound quasi-irreversible to the immobilized ifnar2-EC (Fig. 6A). The ratio between the amounts of ifnar2-EC and 117.7 was 2.5–2.8 throughout various experiments, indicating that each antibody molecule crosslinked two ifnar2-EC molecules. This cooperative interaction substantially reduced dissociation of ifnar2-EC, with a typical loss in IFN-binding capacity of <1% per binding cycle. Immobilized by this method, ifnar2-EC was stable over several days, with a loss in binding capacity of ≤20% per day. The surface was regenerated with a 30-s pulse of 50 mM HCl and could repeatedly be loaded with ifnar2-EC. Thus, a single chip was typically usable for over 1 week. Furthermore, mutants, which were not stable enough to be immobilized by direct covalent coupling, were functionally immobilized by using this technique.

Kinetics of IFN Binding to Immobilized Ifnar2-EC

We used the RIfS system described in this study for a thorough mutational analysis of the binding interface between ifnar2 and IFNα2. This included high-resolution mapping of residues involved in the interaction (17) and double-mutant cycle screening for localizing interactions between individual amino acid residues (unpublished results). Such investigations required accurate quantification of both subtle changes in rate constants and changes in affinity over several orders of magnitude with a high sample throughput. Thus, we thoroughly assessed the potentials and the limitation of the method for biomolecular interaction analysis, as well as potential influence of the immobilization methods.

Rate constants and affinities for the interaction of the wild-type IFNα2 with wild-type ifnar2-EC immo-

TABLE 3

Rate Constants and Affinities of the Interaction of IFNα2 Wild-Type and Ifnar2-EC Determined for Differently Immobilized Ifnar2-EC

Immobilization of ifnar2-EC	IFNα2				IFNβ
	Γ_{max} (pg/mm^2)	k_a (10^6 M^{-1} s^{-1})	k_d (s^{-1})	K_D [nM]	k_d (s^{-1})
Covalent	150–300	2.0 ± 0.4	0.020 ± 0.001	10 ± 2	0.017 ± 0.002
Biotinylated	200–300	3.2 ± 0.5	0.011 ± 0.002	4 ± 1	0.011 ± 0.002
mAb	200–500	3.0 ± 0.5	0.012 ± 0.001	4 ± 1	0.011 ± 0.002

bilized by different methods are compared in Table 3. Covalent immobilization of ifnar2-EC typically gave 150–250 pm (i.e., ~200 pg/mm^2) maximum binding of wild-type IFNα2 (Fig. 5A), which was very suitable for analyzing the binding kinetics. The dissociation kinetics were fit by a single exponential decay with little systematic deviation, indicating a low level of rebinding. The dissociation rate constant for the wild-type proteins was 0.02 ± 0.001 s^{-1} as determined from more than 20 measurements (cf. Table 3). Changes in dissociation rate constants upon mutation down to 20% were resolved with the detection system (17). When ifnar2-EC was biotinylated and then captured on immobilized streptavidin, dissociation was significantly slower with dissociation rate constants of 0.011 ± 0.002 s^{-1} (cf. Fig. 5B and Table 3). A similar, but less pronounced, behavior was observed for IFNβ (Table 3). Essentially the same dissociation rate constant (0.012 ± 0.002 s^{-1}) was measured, when ifnar2-EC was immobilized by affinity capturing (Fig. 5C). For these dissociation curves, significant biasing of single exponential dissociation was observed, which could be attributed to rebinding during dissociation. This phenomenon, however, was not investigated in more detail, but comparison of IFNα2 mutants with different dissociation rate constants confirmed that it depended only on the absolute dissociation rate constants and was not due to the different immobilization techniques (Figs. 7A and 7B). Dissociation rate constants of mutants of IFNα2 and ifnar2-EC discussed in this paper are compared in Table 4. Dissociation rate constants up to 0.3 s^{-1} were clearly resolved by this system as shown in Fig. 7C for IFNα2 wild-type binding to the ifnar2-EC mutant E79A.

Also for the association kinetics, comparable differences for the different immobilization techniques were observed. For the covalently immobilized wild-type ifnar2-EC, an association rate constant of 2.0×10^6 M^{-1} s^{-1} was determined for IFNα2. For the other two immobilization techniques, significantly higher rate constants of 3.2×10^6 M^{-1} s^{-1} for biotinylated ifnar2-EC and of 3.0×10^6 M^{-1} s^{-1} for affinity captured ifnar2-EC were obtained. Immobilization by amine coupling at a pH below the p*I* apparently affects the properties of ifnar2-EC significantly.

By monitoring quenching of tryptophan fluorescence with a stopped flow system, the association rate constant for the IFNα2–ifnar2-EC complex in solution has been determined to be 6.0×10^6 M^{-1} s^{-1} under the same conditions used for solid-phase detection (16). Thus, the association rate constant determined with ifnar2-EC immobilized by affinity capturing was in the same order of magnitude, but still significantly lower. This phenomenon has often been observed when comparing rate constants measured in homogeneous phase and at interfaces and is explained either by interfacial

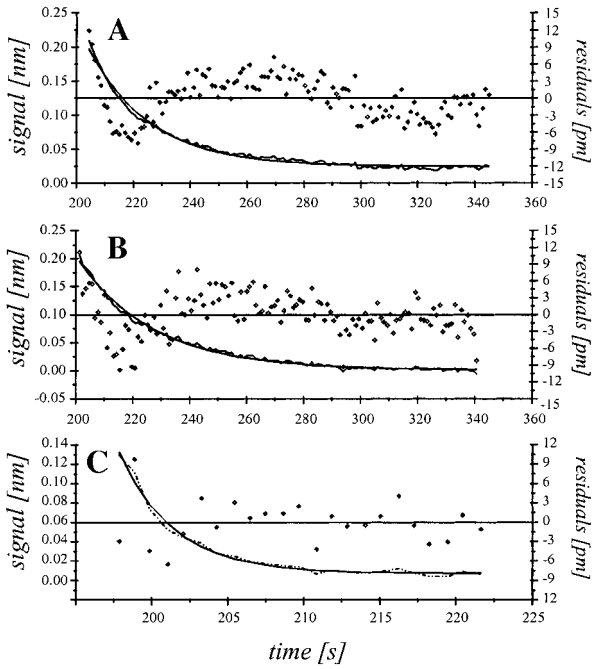

FIG. 7. Fitting of the dissociation kinetics by a single exponential decay. (A) Dissociation of IFNα2 F27A from covalently immobilized wt ifnar2-EC. (B) Dissociation of IFNα2 L153A from wild-type ifnar2-EC immobilized by capturing and crosslinking. (C) Dissociation of IFNα2 wt from ifnar2-EC E79A immobilized by capturing and crosslinking.

mass transport effects (21, 24) or by electrostatic surface potentials (25). Since the association rate constant did not vary for different dextran layers, interfacial mass transport does not seem to play an important role. However, electrostatic attraction was shown to contribute considerably to the formation of the IFNα2–ifnar2-EC-complex (16), suggesting that the second explanation is likely to hold true for this case. Binding curves for the IFNα2–ifnar2-EC interaction indicate significant limitation by diffusion rates (Fig. 8A), which is due to the very fast association rate constant. For the IFNα2 mutant R144A, a substantially lower association rate constant of 3.5×10^5 M^{-1} s^{-1} was determined. Here, no mass transport limitation was observed (Fig. 8B). In agreement with the diffusion parameters discussed above, the limit for association rate constants, which can be determined with this system, is around $2–4 \times 10^6$ M^{-1} s^{-1}.

Dissociation Constants K_D of Low-Affinity Mutants

For mutants with more than a 50-fold decreased affinity, the binding kinetics could not be resolved with this system ($k_d > 0.3$ s^{-1}). The affinities of these mutants were determined from the concentration dependence of the equilibrium binding response as shown in Fig. 9A by fitting Eq. [2]. These dissociation constants

TABLE 4

Rate Constants and Affinities for Some IFNα2 Mutants Binding to Immobilized Ifnar2-EC

IFNα2 mutant	Ifnar2-EC mutant	k_a (10^6 M^{-1} s^{-1})	k_d (s^{-1})	K_D[a] (nM)	K_D[b] (nM)	$\Delta\Delta G^{\ddagger}_{k_d}$[c] (kJ/mol)	$\Delta\Delta G^{0}_{K_D}$[d] (kJ/mol)
wt	wt[e]	3.0	0.012	4	3	—	—
wt	wt[f]	2.0	0.020	10	10	—	—
wt	E79A[e]	2.6	0.31	119	152	8.0	9.9
wt	M48A[e]	—	—	—	3,100	—	17.1
L26A	wt[e]	3.0	0.051	17	31	3.5	4.6
F27A	wt[f]	1.9	0.046	24	n.d.	1.9	—
R33A	wt[e]	—	—	—	27,900	—	22.4
R144A	wt[e]	0.35	0.048	136	117	3.3	9.3
R149A	wt[e]	—	—	—	470	—	12.6
R149A	M48A[e]	—	—	—	198,000	—	—
L153A	wt[e]	3.2	0.10	31	44	5.2	6.9

Note. Ifnar2-EC was immobilized via antibodies if not stated otherwise.
[a] Determined from the rate constants according to Eq. [1].
[b] Determined from the equilibrium response according to Eq. [2].
[c] Determined from the dissociation rate constant k_d according to Eq. [5].
[d] Determined from the dissociation constant K_D according to Eq. [4].
[e] Ifnar2-EC captured to the surface by immobilized mAbs.
[f] Ifnar2-EC directly immobilized to the surface by amide coupling.

K_D were in good agreement with the K_D determined from the rate constants according to Eq. [1] for all mutants, for which the rate constants could be resolved, independent of the immobilization technique (cf. Table 4).

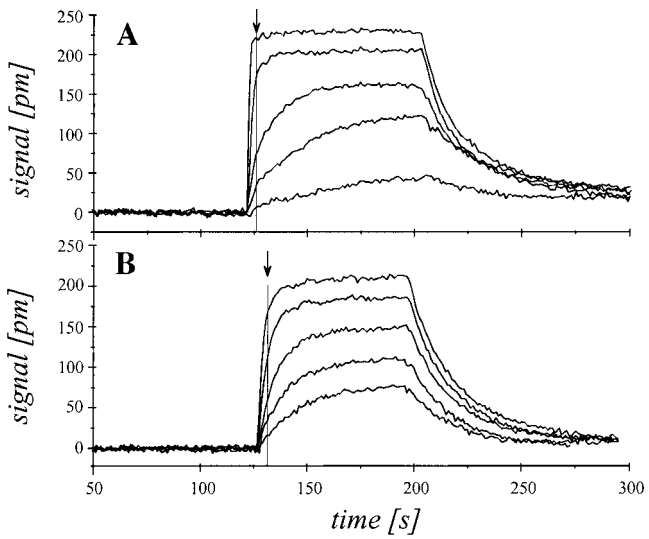

FIG. 8. BIA of two different IFNα2 mutants with comparable dissociation rate constants (cf. Table 4) binding to immobilized wild-type ifnar2-EC. (A) Binding curves for the mutant L26A at concentrations of 5, 20, 50, 200, and 1000 nM. Mass transport limitations are obvious from the abrupt decrease of the slope when changing the flow rate after the fast injection as indicated by the arrow. An association rate constant of $k_a = 3 \times 10^6$ M^{-1} s^{-1} like for wild-type IFNα2 was determined. (B) Binding of the IFNα2 mutant R144A at concentrations of 10, 30, 100, 300, and 1000 nM. No mass transport limitation is observed, with an association rate constant of $k_a = 3.5 \times 10^5$ M^{-1} s^{-1}.

For the determination of the K_D from the equilibrium coverage, the maximum binding signal (R_{max}) is a parameter of critical importance, as it defines the relative occupancy of the binding sites (R_{eq}/R_{max}). In cases of mutants with very low affinities, R_{max} was not reached with concentrations up to 50 μM. For these mutants, the R_{max} determined from a fit of a higher-affinity mutant was used, as demonstrated in Fig. 9B for the mutant IFNα2 R33A binding to wild-type ifnar2-EC. Using the R_{max} determined for the IFNα2 mutant L153A, the K_D was determined to be 31 μM.

Because of the fast, transient interaction at very low affinity binding ($k_d > 0.5$ s^{-1}), background signals cannot be discriminated from the binding signal and thus can critically affect the result. Therefore, we investigated the reliability and the limits of the system by analyzing the interaction between a low-affinity mutant of ifnar2-EC (M48A, $K_D = 3.4$ μM) and the low-affinity mutants R33A and R149A of IFNα2. For R33A, no binding was detected at 50 μM concentration (i.e., 1 mg/ml protein), indicating that the affinity between these two mutants is too low to promote significant complex formation at this concentration. The absence of any signal impressively proves that neither background signal nor nonspecific binding interferes with the binding signal even at this extremely high protein concentration. With SPR detection, a background signal around the maximum binding R_{max} is expected for this protein concentration (188 RU for 1 mg/ml protein). For the mutant R149A, a response of 40 pm was observed on immobilized M48A (Fig. 9B), corresponding to a dissociation constant of 200 μM. Since signals down to 20 pm can be clearly detected and quantified,

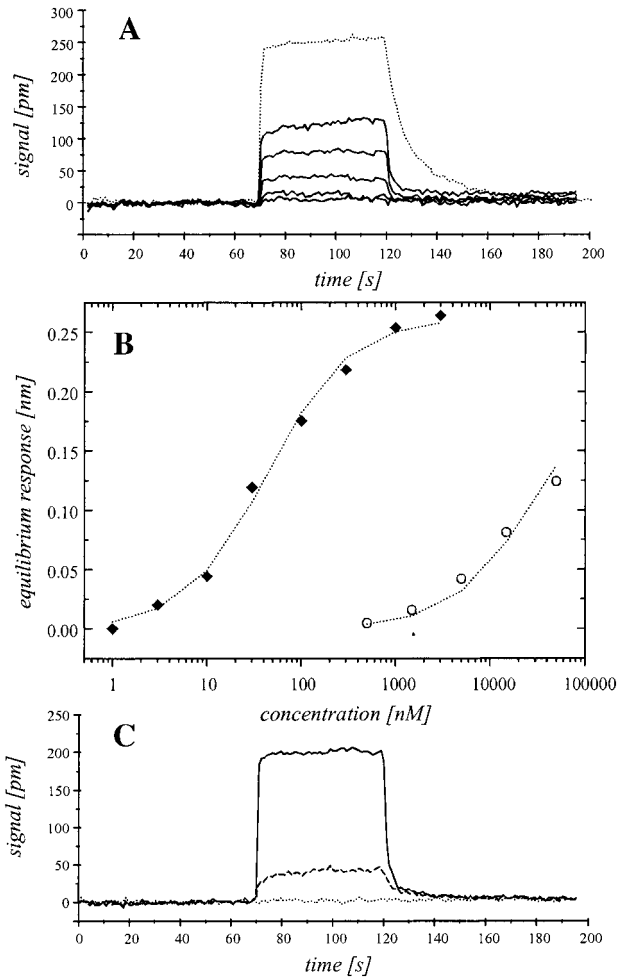

FIG. 9. Affinity analysis of mutants with very low affinities (K_D > 10 μM). (A) Binding of IFNα2 R33A in different concentrations (0.3, 1, 3, 10, and 30 μM) on wt ifnar2-EC (—) and maximum loading determined with 3 μM IFNα2 L153A (···). (B) Secondary plot comparing the concentrations dependence of the equilibrium binding signals for IFNα2 L153A (◆) and R33A (○), and the Langmuir fit to the data points (···). (C) Binding of 50 μM IFNα2 R33A (···), 50 μM IFNα2 R149A (- - -), and 30 μM wild-type IFNα2 (—) on ifnar2-EC M48A.

minimum affinities of ~500 μM could be detected. Thus, changes over 5 orders of magnitude compared to the wild-type affinity of 3 nM were quantified. By using protein concentrations higher than 50 μM, even lower affinity should be detectable, but this was not investigated.

Comparison of ΔΔG upon Mutation

Important for mutational analysis of protein–protein interactions is the possibility for a precise mapping of relative changes in kinetic or thermodynamic parameters. Since different absolute values were obtained when using different immobilization techniques, we compared the changes in free energy upon mutation (both $\Delta\Delta G^0_{K_D}$ and $\Delta\Delta G^{\ddagger}_{k_d}$) obtained for the different immobilization methods. In Fig. 10A, this comparison is shown for covalently immobilized ifnar2-EC and for antibody-immobilized ifnar2-EC (wild type in both cases). Linear correlation was observed for both IFNα2 and ifnar2-EC mutants, with a slope of 1.1 ± 0.04 (r = 0.996) and 1.00 ± 0.04 (r = 0.994), respectively. These results corroborate that relative changes in kinetics and affinity are independent of the immobilization method and can be precisely quantified by solid-phase detection.

DISCUSSION

BIA based on label-free solid-phase detection is a powerful approach for characterizing kinetics and thermodynamics of protein–protein interaction and is, for its versatility, particularly useful in mutational analysis. Additional to the detection system and suitable sample handling, surface modification and protein immobilization are the main challenges for establishing systems useful for BIA. Here, we have employed a transducer based on directional reflection to set up a system capable of automated flowthrough BIA and established efficient methods to specifically monitor protein–protein interactions. In contrast to evanescent field techniques, which probe a given region adjacent to the surface, this transducer selectively interrogates the layer involved in the interaction. Background signals and temperature-dependent fluctuations are therefore tremendously lower, allowing for a very simple and rugged setup without temperature stabilization or reference channels. However, the detection limit of 5–10 pg/mm^2 is approximately 1 order of mag-

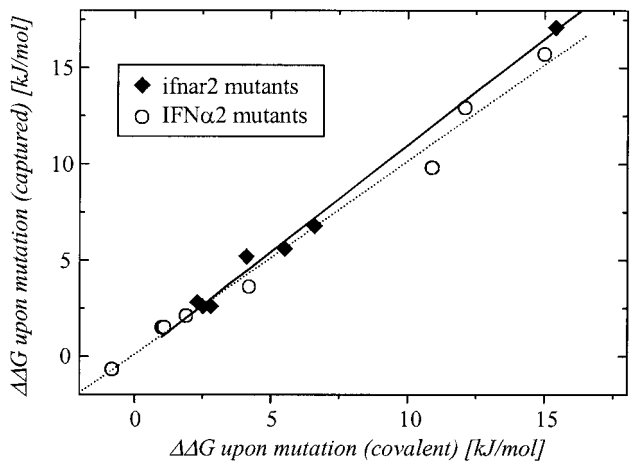

FIG. 10. Comparison of the change in free energy of comlex formation ($\Delta\Delta G^0_{K_D}$ and $\Delta\Delta G^{\ddagger}_{k_d}$) for various mutations on IFNα2 (○) and ifnar2-EC (◆), obtained by covalent immobilization of ifnar2-EC and by capturing and crosslinking with anti-ifnar2-EC mAbs.

nitude higher than for the highly optimized BIAcore2000 system (~1 pg/mm^2).

We established methods for surface modification suitable for the silica surface of this interferometric transducer and for functional protein immobilization. Carboxy-methylated dextran layers on gold surfaces covered with hydroxy-terminated self-assembled monolayers have been very successfully applied for protein immobilization (22). Chemical modification of glass-type surfaces, however, requires different approach from the modification of gold surfaces for two reasons: First, protection of the surface with hydroxy-terminated self-assembled monolayers is not readily achieved as it is on gold. Thus, an alternative strategy for shielding surface against nonspecific binding was required. Second, silica chemistry quickly decomposes in alkaline environment, and therefore acidic to neutral reaction conditions are required. Direct coupling of dextran to surfaces activated with epoxy-functional silanes under neutral conditions is difficult to control and yields low dextran loadings (26, 27) (and unpublished results). For more efficient coupling, we used dextrans functionalized with amine groups. Coupling of these AMD by amide chemistry was very efficient, but critical because of considerable nonspecific binding to the aminosilane used for surface activation (19, 28). Recently, we showed a significant decrease in nonspecific binding by using GOPTS for silanization, which was even more improved by coupling a thin, dense layer of bifunctional PEG (18). We used these strategies for preparing dextran layers with different polymer loadings and protein-binding capacities, which all showed very low nonspecific binding and allowed versatile application for the immobilization of different proteins. Interestingly, background effects severely increased with increasing amount and extension of the polymer being immobilized. This important fact must be taken into account for the design of optimum surface chemistry. A principal advantage of this surface chemistry is that the transducers can be reused after selectively removing the attached layers by treatment with NaOH and piranha solution, thus tremendously reducing operation costs.

We investigated the potential of this biosensor system for structure–function analysis of a cytokine–receptor interaction by site-directed mutagenesis. The binding of IFNα2 to the extracellular domain of its receptor ifnar2 immobilized on the transducer surface was monitored in real time. Comparing different methods of immobilization of ifnar2-EC revealed significant differences in kinetics and affinity of IFNα2 binding. Direct covalent coupling of the protein most strongly affected the interaction properties. Compared to immobilization by affinity capturing, the affinity was decreased both by a decrease in the association rate constant and by an increase in the dissociation rate constant. Furthermore, heterogeneous affinity of the immobilized ifnar2-EC was observed. This effect was attributed to heterogeneous association rate constant, while the dissociation rate constant appeared homogeneous for the total amplitude. Very similar results have been obtained by using a BIAcore 2000 system for these investigations (16). These effects were not observed for biotinylated ifnar2-EC captured by immobilized streptavidin, where also amines moieties of the proteins were randomly used for attachment. Hence, the critical factor lies in the coupling conditions, which requires a pH below the pI of the rather acidic proteins to achieve electrostatic preconcentration. While the protein was not damaged at this pH in solution (data not shown), covalent coupling under these conditions affects its function. Though relative parameters such as $\Delta\Delta G$ upon mutation were in good agreement with other immobilization techniques, the direct covalent attachment was not reliable for the characterization of mutants with low affinity.

For reversible immobilization, we devised a new strategy for antibody-based affinity capturing. Crosslinking ifnar2-EC captured with an immobilized high-affinity mAb with a second, noncompetitive mAb proved to effectively reduce leaking out, while the possibility to nondestructively remove the immobilized protein was maintained. Thus, stable, but reversible attachment of ifnar2-EC was achieved, allowing for analysis of many different ifnar2-EC mutants on the same surface, including mutants with lower stability than the wild-type protein. The principal concept of avidity-based stabilization of affinity-captured proteins presented here provides a promising generic approach for reversible affinity capturing.

Quantitative mutational analysis particularly requires a wide dynamic range of affinities to be measurable, because single mutations can destabilize protein–protein complexes by several orders of magnitude (1, 2). Biomolecular interaction analysis with numerous mutants of IFNα2 and ifnar2-EC located in the interface of the complex allowed for a thorough analysis of the limits of the system with respect to resolution of rate constants and lowest affinities to be quantified. Determination of rate constants is limited by parameters related to the sample handling. The maximum dissociation rate constant is determined by the time needed to remove the sample from the flow cavity. Here, we determined a limit of ~0.3 s^{-1} given by a time constant of ~1 s^{-1} for rinsing the cell, which is in the range what has been achieved by microfluidics (29). For one IFNα2 mutant, a dissociation rate constant of 0.3 s^{-1} was determined with a standard deviation of approximately 20%, proving the practical significance of these values. Maximum association rate constants are typically limited by mass transport to the surface. We found significant influence of mass transport for an

association rate constant of $3.0 \times 10^6 M^{-1} s^{-1}$, which was not observed for an approximately ninefold lower association rate constant of $3.5 \times 10^5 M^{-1} s^{-1}$. Thus, a typical limit of $1–5 \times 10^6 M^{-1} s^{-1}$ for the determination of association rate constants with this system is estimated. Particular impressive results were obtained for the determination of affinity constants from equilibrium-binding signals. This method tremendously profited from the advantages of RIfS detection and the advanced surface chemistry: up to protein concentration of 50 μM IFNα2, neither nonspecific binding nor background signals interfered with detection, allowing quantification of affinities of protein interactions up to 200 μM and probably even higher. Thus, affinities over 5 orders of magnitude were assessed, which proved to be extremely valuable for double mutant cycle analysis of protein–protein interaction.

The simple and rugged experimental setup, the versatile surface chemistry, and the suitability for low-affinity interaction analysis makes RIfS technology an attractive tool for functional characterization of binding interfaces by mutational analysis. Its performance in terms of detection limits and time resolution is clearly competitive with established systems, while it provides major advantages due to high stability, low background, and, not least, low costs. The major potential for improvement of the system lies in a miniaturization of the sample handling, by which sample consumption could be effectively reduced, and the stability and mass transport rates could be increased.

ACKNOWLEDGMENTS

The authors are grateful to Hans-Martin Haake from the group of Günter Gauglitz, University of Tübingen, for supporting setting up and maintaining the RIfS system both by materials and advice. The anti-ifnar2-EC mAbs 46.10 and 117.7 were a gift from Daniela Novick at the Weizmann Institute of Science. Ellipsometric and contact angle measurements were carried out with the kind support by Ramûnas Valiokas in the group of Bo Liedberg, Linköpings University. This work was supported by Grant 96-00439/1 from the US–Israel Binational Science Foundation (BSF). J.P. was an EMBO postdoctoral fellow, 1998–1999. G.S. is incumbent of the Dewey David Stone and Harry Levine career development chair.

REFERENCES

1. Cunningham, B. C., and Wells, J. A. (1993) Comparison of a structural and a functional epitope. *J. Mol. Biol.* **234,** 554–563.
2. Schreiber, G., and Fersht, A. R. (1993) Interaction of barnase with its polypeptide inhibitor barstar studied by protein engineering. *Biochemistry* **32,** 5145–5150.
3. Albeck, S., and Schreiber, G. (1999) Biophysical characterization of the interaction of the β-lactamase TEM-1 with its protein inhibitor BLIP. *Biochemistry* **38,** 11–21.
4. Schreiber, G., and Fersht, A. R. (1995) Energetics of protein–protein interactions: Analysis of the barnase–barstar interface by single mutations and double mutant cycles. *J Mol. Biol.* **248,** 478–486.
5. Albeck, S., Unger, R., and Schreiber, G. (2000) Evaluation of direct and cooperative contributions towards the strength of buried hydrogen bonds and salt bridge. *J. Mol. Biol.* **298,** 503–520.
6. Karlsson, R., Michaelsson, A., and Mattson, L. (1991) Kinetic analysis of monoclonal antibody–antigen interactions with a new biosensor based analytical system. *J. Immunol. Methods* **145,** 229–240.
7. Fägerstam, L. G., Frostell-Karlsson, A., Karlsson, R., Persson, B., and Rönnberg, I. (1992) Biospecific interaction analysis using surface plasmon resonance detection applied to kinetic, binding site and concentration analysis. *J. Chromatogr.* **597,** 397–410.
8. Edwards, P. R., Gill, A., Pollard-Knight, D. V., Hoare, M., Buckle, P. E., Lowe, P. A., and Leatherbarrow, R. J. (1995) Kinetics of protein–protein interactions at the surface of an optical biosensor. *Anal. Biochem.* **231,** 210–217.
9. Nieba, L., Krebber, A., and Plückthun, A. (1996) Competition BIAcore for measuring true affinities: Large differences from values determined from binding kinetics. *Anal. Biochem.* **234,** 155–165.
10. Nieba, L., Nieba-Axmann, S. E., Persson, A., Hamalainen, M., Edebratt, F., Hansson, A., Lidholm, J., Magnusson, K., Karlsson, A. F., and Plückthun, A. (1997) BIACORE analysis of histidine-tagged proteins using a chelating NTA sensor chip. *Anal. Biochem.* **252,** 217–228.
11. Karlsson, R., and Stahlberg, R. (1995) Surface plasmon resonance detection and multi-spot sensing for direct monitoring of interactions involving low-molecular-weight analytes and for determination of low affinities. *Anal. Biochem.* **228,** 274–280.
12. Brecht, A., and Gauglitz, G. (1995) Optical probes and transducers. *Biosens. Bioelectron.* **10,** 923–936.
13. Brecht, A., Gauglitz, G., and Polster, J. (1993) Interferometric immunoassay in a FIA-system: A sensitive and rapid approach in label-free immunosensing. *Biosens. Bioelectron.* **8,** 387–392.
14. Schmitt, H.-M., Brecht, A., Piehler, J., and Gauglitz, G. (1997) An integrated system for optical biomolecular interaction analysis. *Biosens. Bioelectron.* **12,** 809–816.
15. Piehler, J., Brecht, A., and Gauglitz, G. (1996) Affinity detection of low molecular weight analytes. *Anal. Chem.* **68,** 139–143.
16. Piehler, J., and Schreiber, G. (1999) Biophysical analysis of the human type I interferon receptor ifnar2 expressed in *E. coli* with interferon α2. *J. Mol. Biol.* **289,** 57–67.
17. Piehler, J., and Schreiber, G. (1999) Mutational and structural analysis of the binding interface between type I interferons and their receptor ifnar2. *J. Mol. Biol.* **294,** 223–237.
18. Piehler, J., Valiokas, R., Liedberg, B., Brecht, A., and Gauglitz, G. (2000) A high-density PEO polymer brush for immobilization on glass-type surfaces. *Biosens. Bioelectron.***15,** 473–481.
19. Piehler, J., Brecht, A., Hehl, K., and Gauglitz, G. (1999) Protein interactions in covalently attached dextran layers. *Colloids Surf. B: Biointerfaces* **13,** 325–336.
20. Gauglitz, G., Brecht, A., Kraus, G., and Nahm, W. (1993) Chemical and biochemical sensors based on interferometry at thin (multi-)layers. *Sens. Actuators B* **11,** 21–27.
21. Glaser, R. W. (1993) Antigen–antibody binding and mass transport by convection and diffusion to a surface: A two-dimensional computer model of binding and dissociation kinetics. *Anal. Biochem.* **213,** 153–161.
22. Löfas, S., and Johnsson, B. (1990) A novel hydrogel matrix on gold surfaces in surface plasmon resonance sensors for fast and efficient covalent immobilisation of ligands. *J. Chem. Soc. Chem. Commun.* **1990,** 1526–1528.

23. Cohen, B., Novick, D., Barak, S., and Rubinstein, M. (1995) Ligand-induced association of the type I interferon receptor components. *Mol. Cell Biol.* **15,** 4208–4214.

24. Schuck, P., and Minton, A. P. (1996) Analysis of mass transport-limited binding kinetics in evanescent wave biosensors. *Anal. Biochem.* **240,** 262–272.

25. Leckband, D. E., Kuhl, T., Wang, H. K., Herron, J., Muller, W., and Ringsdorf, H. (1995) 4–4–20 anti-fluorescyl IgG Fab′ recognition of membrane bound hapten: Direct evidence for the role of protein and interfacial structure. *Biochemistry* **34,** 11467–11478.

26. Elam, J. H., and Nygren, H. (1984) Covalent coupling of polysaccharides to silicon and silicon rubber surfaces. *J. Biomed. Mater. Res.* **18,** 953–959.

27. Elender, G., Kühner, M., and Sackmann, E. (1996) Functionalisation of Si/SiO_2 and glass surfaces with ultrathin dextran films and deposition of lipid bilayers. *Biosens. Bioelectron.* **11,** 565–577.

28. Piehler, J., Brecht, A., Geckeler, K. E., and Gauglitz, G. (1996) Surface modification for direct immunoprobes. *Biosens. Bioelectron.* **11,** 579–590.

29. Sjölander, S., and Urbaniczky, C. (1991) Integrated fluid handling system for biomolecular interaction analysis. *Anal. Chem.* **63,** 2338–2345.